Journal of Environmental Chemical Engineering 12 (2024) 113071

Contents lists available at ScienceDirect

Journal of Environmental Chemical Engineering

journal homepage: www.elsevier.com/locate/jece

Comparative study of bioanodes for microbial electrolysis cells operation in anaerobic digester conditions

Simone Colantoni [a], Óscar Santiago [a], Janek R. Weiler [b], Melanie T. Knoll [b], Christian J. Lapp [b], Johannes Gescher [b], Sven Kerzenmacher [a,*]

[a] University of Bremen, Center for Environmental Research and Sustainable Technology (UFT), Research Group Environmental Process Engineering, Leobener Str. 6, Bremen 28359, Germany

[b] Institute of Technical Microbiology, Hamburg University of Technology, Kasernenstraße 12, Hamburg 21073, Germany

ARTICLE INFO

Keywords:
Microbial electrolysis cell
Material selection
Bioanode stability
Anode material screening
Anaerobic digestion
Electrodes biodiversity

ABSTRACT

Integrating microbial electrolysis cells (MEC) with anaerobic digestion (AD) would offer different synergistic advantages to these technologies. The MEC bioanode could be immersed in the AD reactor, stabilizing the process, or operated as an independent cell, further removing organic matter. However, up to now, bioanodes operated in anaerobic digestion conditions present low current production and tend to deactivate over time. In the present work, we conducted a comparison of six carbon-based and metal-based electrode materials, including novel options such as stainless steel wool (SSW) and carbon nanofibers (ES300), never tested before under these conditions. The electrodes were evaluated using two inoculation procedures, operating simultaneously in the same electrolyte with different feeding media. The bioanodes produced double the current densities when fed with undigested corn silage compared to anaerobic digester effluent, showing the potential for direct integration into anaerobic digesters without pre-fermentation. Unprecedented stable current densities, up to 0.4 mA cm^{-2}, were obtained over 60 days of operation in real anaerobic digestion conditions by *Geobacter*-dominated bioanodes on SSW and ES300, outperforming state-of-the-art bioanodes and avoiding the dramatic deactivation previously reported. Microbial community analysis of SSW and ES300 elucidated how the microbial composition in the bioanodes was mostly depending on the electrode material, rather than the inoculation procedure. The results achieved with these bioanodes pave the way for scaling up and commercializing integrated AD-MEC systems.

1. Introduction

Anaerobic digestion (AD) is a well-established bioprocess for the sustainable treatment of organic matter and energy recovery. Here, complex organic substances like silage and other agricultural waste, animal manure, food waste, and wastewater get consumed by a mixed microbial community in anaerobic conditions producing biogas, a mixture of methane and carbon dioxide [1,2]. Coupling an anaerobic digester with a microbial electrolysis cell (MEC), where electroactive microorganisms consume small organic molecules (e.g., organic acids) and utilize a polarized electrode as an electron acceptor for their respiration metabolism [3], offers several synergetic advantages to the AD process, as described in recent reviews [4]. For instance, a MEC can stabilize an anaerobic digester in case of organic acids and nitrogen overloads [5], improve the methane content of the biogas, and recover ammonium [6], while the chemical oxygen demand (COD) of the anaerobic digester medium can provide part of the energy necessary for the MEC operation.

The core of a microbial electrolysis cell is the so-called bioanode, where the interaction between the electrode material and the electroactive biofilm (EABf) takes place [7,8]. EABf grows on the surface of polarized electrodes and uses them as electron acceptors in their metabolism [9]. To form an EABf on an electrode surface, usually an inoculation with a source of electroactive microorganisms is required, either in pure culture, defined-mixed culture, or with natural inoculum sources (i.e., activated sludge, wastewaters, anaerobic sludge). According to several reviews [10–12], the main type of electrode utilized are carbon-based materials [11] such as graphite felt, carbon paper and graphite plates, and stainless steel-based materials, which can provide excellent performances as bioanodes [12,13], even outperforming

* Corresponding author.
E-mail address: kerzenmacher@uni-bremen.de (S. Kerzenmacher).

https://doi.org/10.1016/j.jece.2024.113071
Received 15 December 2023; Received in revised form 10 May 2024; Accepted 13 May 2024
Available online 14 May 2024

carbon-based ones [14]. However, most studies of bioanodes are performed in independent biological experiments, where the bioanodes are inoculated and operated independently from each other. This brings a bias due to the differences in the inoculation procedure and from the intrinsic heterogeneity of complex organic substrates, which change dynamically their conditions (e.g. pH, type, and concentration of organic compounds) due to fermentation, making it difficult to have the same conditions in different bioreactors [15,16]. In this sense, only a few systematic comparative studies of materials operated simultaneously in the same medium are reported in literature [14,17,18], and a robust comparative methodology for benchmarking different bioanode is still lacking in the field.

In addition to this, the current densities and long-term stability of bioanodes operated in industrially relevant conditions (i.e. with complex non-axenic media as the electrolyte and without additional carbon sources) are usually significantly lower than the ones reported for bioanodes operated in acetate media and axenic conditions [19]. The development of high-performing bioanodes, capable of achieving long-term high current densities, is considered one of the main requirements for MEC scalability and industrial application [20]. In this regard, Rosa *et al.* [21] reported a maximum current density of 0.01 mA cm^{-2} for bioanodes developed on graphite rods without pre-enrichment and operated in amendment-free wastewater. Madjarov *et al.* [22] showed how anodes inoculated with a defined mix community of *Geobacter sulfurreducens*, *Geobacter metallireducens,* and *Shewanella oneidensis* performed similarly as non-inoculated anodes and anodes inoculated with sewage sludge when operated with municipal wastewater as substrate. Christgen *et al.* [19] presented a comparison of different bioanodes developed on carbon veil as electrode material utilizing three different inoculum sources and pre-enriched in acetate media. Regardless of the inoculum used, all bioanodes showed a drop in current densities, going from 0.25 to 0.45 mA cm^{-2} in acetate media to around 0.1 mA cm^{-2} when the acetate media was exchange to domestic wastewater [19]. Kretzschmar *et al.* [23] showed how fully matured *Geobacter* spp. EABf on graphite rod electrodes lost their functionality within 1–8 days when operated inside an anaerobic digester. These results were expanded later by Dzofou Ngoumelah *et al.* [24], who showed how older *Geobacter* spp. dominated EABf developed on graphite rods had higher performances and resistance to deactivation in anaerobic digestion conditions compared to younger ones. In any case, even the older EABf showed a severe loss in current production during stepwise adaptation to AD effluent.

From the results reported in literature, it appears that the improvement of the current densities achievable by bioanodes in realistic industrial conditions is still a major necessity for the industrial application of MEC [20]. In this sense, the aim of this paper is to develop bioanodes capable of long-term high current density production, as well as investigate the interdependency between electrode materials, inoculation procedures and fermentation degree of the feeding substrate, and their effects on the electrochemical response of bioanodes operating in complex, non-axenic anaerobic digester media. For this purpose, we carried out a cross-comparison between commercially available electrode materials (graphite felt, graphite plate, stainless steel plate, stainless steel mesh) and novel electrode materials which were never tested before as bioanodes in anaerobic digester conditions (stainless steel wool and in-house produced carbon nanofibers CNF-ES300). The bioanodes were operated simultaneously and immersed in the same medium (overcoming the bias of independent biological experiments) in two independent reactors inoculated with either a mixed culture of *G. sulfurreducens* and *S. oneidensis* or with a natural consortium from an 8 L laboratory-scale anaerobic digester digesting corn silage. The electrochemical performances of the bioanodes were characterized by chronoamperometry and polarization curves during the stepwise adaptation to the effluent from the same laboratory-scale anaerobic digester, and afterward to the undigested corn silage which was used as feeding substrate for the same laboratory-scale anaerobic digester. The daily bioreactor conditions (pH, conductivity, organic acids concentration, soluble chemical oxygen demand) were monitored. Additionally, metagenomic analysis of the best-performing bioanodes were performed at the end of the experimentation, to better understand the influence of electrode materials and pre-inoculation procedures on the microbial bioanode composition.

This work reports the development of *Geobacter*-dominated bioanodes on stainless steel wool and carbon nanofibers capable of achieving unprecedented and stable current densities for over two months of operation under real anaerobic digestion conditions, up to 0.4 mA cm^{-2}, representing a four-fold increase compared to previously reported results. It is also elucidates how the right choice of electrode material and inoculation procedure enables the development of bioanodes with improved long-term stability and current production in an anaerobic digester environment, overcoming challenges that, until now, where only tackle from the point of view of the biological engineering of the bioelectrodes [19,24,25]. Moreover, the reported methodology represents a step ahead for the implementation of solid cross-comparative methodologies in the field.

2. Materials and methods

2.1. Chemicals, materials, and methods

All the chemicals used were analytical grade or higher and were used as received. A gas mixture consisting of 20% mol CO_2 (purity $\geq$ 99.995%, Linde, Germany) and 80% mol N_2 (purity $\geq$ 99.999%, Air Liquide, Germany) was used for purging and anaerobization. The pH measurements were done with a SenTix Mic probe connected to a Multiline P4 measurement device (Xylem Analytics Germany GmbH, Germany). Conductivity measurements were done with a WTW TetraCon 325 probe connected to a Multiline P4 measurement device (Xylem Analytics Germany GmbH, Germany).

Soluble chemical oxygen demand (COD) was determined using Hach-Lange cuvette kits LCK014 with a detector model DR 3900 (Hach-Lange, Germany) after sample filtration on 0.2 μm surfactant-free cellulose acetate filters (Sartorius, Germany). The same detector was used also to measure the optical density at a wavelength of 600 nm (OD_{600}). The total COD was determined using the same procedure as the soluble COD but without the filtration step. To track the organic acid concentrations, high-performance liquid chromatography (HPLC) measurements were performed in an HPLC system (Alliance, Waters, Germany) with 2414 refractive and 2489 UV index detectors (Waters, Germany) equipped with an Aminex HPX-87 H column (300 × 7.8 mm) with 8 mM H_2SO_4 as eluent at 0.6 mL/min and column at 35 °C.

All the potentials throughout this work are referred to an Ag/AgCl electrode model SE20EB (sat. KCl, 197 mV vs. Standard hydrogen electrode, Sensortechnik Meinsberg, Xylem Analytics Germany GmbH, Germany). The electrochemical analysis (chronoamperometry, polarization curves, linear sweep voltammetry) were carried out using either a multichannel potentiostat model PGU-MOD 500 mA-4 K (IPS Elektroniklabor GmbH and Co., KG, Germany) or single-channel potentiostat Gamry Interface 1010 (GAMRY Instruments, USA).

2.2. Media preparation

The anode medium, containing lactate as the only organic substrate, was derived from [26] and is reported in Table S1. *S. oneidensis* produces acetate from lactate, providing a constant acetate feed to *G. sulfurreducens* in co-culture conditions [27]. The undigested corn silage was prepared weekly by mixing with a blender 80 g L^{-1} of frozen solid corn silage, 2.65 g L^{-1} of Na_2CO_3, 0.25 g L^{-1} of NH_4Cl, and 1 mL L^{-1} of trace element solution (reported in Table S2) in distilled water and kept aerobic at 4 °C in a fridge. The solid corn silage was obtained from a full-scale biogas plant, and it was autoclaved and kept frozen at −20 °C. The undigested corn silage and the anaerobic digester

effluent (ADE) were sieved aerobically on 2×2 mm stainless steel mesh before feeding to the reactors. The ADE was obtained from a laboratory-scale anaerobic digester, inoculated with 10% V/V media from a full-scale biogas plant, and digesting the previously described undigested corn silage at an organic loading rate (OLR) of 1.33 gO_2 $L_{reactor}^{-1}$ d^{-1} with a hydraulic retention time of 40 days.

2.3. Inoculum sources

G. sulfurreducens PCA was cultivated in an anaerobic medium for 48 hours as described by Coppi *et al.* [28]. After cultivation, the cells were centrifugated and washed three times to remove soluble electron acceptors, following the procedure described by Kipf *et al.* [17]. *S. oneidensis* MR-1 was cultivated as described elsewhere [18,29] and washed three times before inoculation to remove soluble electron acceptors. The natural mixed microbial community was obtained from the laboratory scale anaerobic digester and sieved on 2×2mm stainless steel mesh before inoculation.

2.4. Experimental set-up

The information regarding the electrode materials tested are reported in Table 1. All the materials were commercially available except for the carbon nanofibers ES300 (CNF-ES300). These were fabricated by electrospinning of 8 wt% polyacrylonitrile in N,N-dimethylacetamide and subsequent carbonization at 1000 °C, following the procedure reported by Erben *et al.* [30]. The experiments were carried out at a controlled temperature of 35 °C in two battery glass reactors (BGRs) adapted from Erben *et al.* [31] under continuous purging with a 20/80 mol% CO_2/N_2 gas mixture and continuous stirring at 300 rpm with a magnetic stirrer. The reactors were made anaerobic *via* gas purging 24 hours before the inoculation and were utilized without any prior sterilization. All the electrode materials had a projected surface area of 2.25 cm^2 and were assembled as described by Vázquez *et al.* [14]. Platinized titanium meshes (2.5 μm Pt layer, 1 mm thickness, Horbach Industriebedarf GmbH, Idar-Oberstein, Germany) with a projected surface area of 2.25 cm^2 were used as counter electrodes for each working electrode. Titanium gauze (60 mesh woven from 0.2 mm diameter wire, Alfa Aesar, Germany) was used as the current collector for each of the working electrodes, while titanium wire (99.7 wt%, 0.25 mm diameter, Sigma Aldrich, Germany) was used as the current collector for the counter electrodes and for the electrical connection between the current collectors and the external connections to the potentiostat.

Table 1
Electrode materials information.

Material	Type	Thickness	Manufacturer
Graphite Plate (GP)	MR40	3 mm	Müller & Rössner GmbH & Co. KG, Troisdorf, Germany
Graphite felt (Felt)	GFD 2.5 EA	2.5 mm	SGL Carbon SE, Wiesbaden, Germany
Carbon nanofiber mat (CNF-ES300)	ES300	≈ 0.7 mm	In-house fabrication [30]
Stainless steel plate (SSP)	EN 1.4301	1 mm	EMB-Edelstahl & Metallhandelsgesellschaft GmbH, Stuhr, Germany
Stainless steel mesh (SSM)	EN 1.4301 w = 0,5 mm d = 0,4 mm	1 mm (from wire diameter)	HAVER & BOECKER OHG, Oelde, Germany
Stainless steel wool (SSW)	EN 1.4113 d ≈ 0.09 mm	≈ 3 mm	RAKSO, Oscar Weil GmbH, Lahr, Germany

2.5. Experimental procedure

Two 960 mL BGRs were operated simultaneously following the same experimental strategy, the only difference being the inoculation procedure. The first bioreactor, denominated "BGR-GS", was inoculated with *G. sulfurreducens* at an OD_{600} of 0.01 and *S. oneidensis* at an OD_{600} of 0.09 and kept in open circuit potential (OCP) for two days before the start of the chronoamperometry (CA). This strategy was followed to allow the bacteria to establish themselves on the anode surface before the application of an external potential. The second bioreactor, denominated "BGR-NMC", was inoculated with the natural mixed microbial community from the lab-scale anaerobic digester in a ratio of 1% V/V. BGR-NMC was polarized immediately after inoculation, to prevent the anode colonization by non-electroactive microbes (e.g., fermenters, methanogens) present in vast majority in the inoculum [32–35].

Both BGRs were operated in chronoamperometry mode at a set potential of −197 mV vs Ag/AgCl (0 mV vs SHE) [14]. The chronoamperometry was only interrupted for the recording of the polarization curves (PC) and restarted immediately after. PC were used to obtain voltage-current behaviour for the electrodes in different media conditions over time and were performed immediately after feeding the reactors, according to the procedure described as follows [14]: after 1 hour of equilibration at −197 mV vs Ag/AgCl, the OCP of the electrodes was recorded for 30 minutes. Afterward, the potential was increased from −405 mV vs. Ag/AgCl to 45 mV vs. Ag/AgCl in 50 mV steps every 30 minutes, with a recording time of one point every second. The current densities were obtained from the average of the last 100 points of each potential step [14]. The charge exchanged, expressed in coulombs normalized by the electrode area (C cm^{-2}), was calculated as the integral of the chronoamperometry in the two days before and after each PC, as shown in Eq. 1.

$$C = \int_{t_1}^{t_2} I dt \tag{1}$$

Due to the low conductivity of the media (in the range 5–7 mS cm^{-1}) and the distance between the reference electrode and the working electrodes, the bioanodes' potentials during the chronoamperometry and polarization curves were corrected considering the uncompensated resistance (iR_u-drop) using the procedure reported by Madjarov *et al.* [36]. For this work, the reported potentials were corrected using Eq. 2 [14,36].

$$E_{calc} = E_{app} - \frac{K_r I}{\sigma} \tag{2}$$

where E_{calc} is the corrected potential of the electrode, E_{app} is the potential applied by the potentiostat, without correction, I is the current produced by the bioanode, σ is the conductivity of the medium and K_r is the geometry factor of the reactor. For the reactor design utilized in this work, a geometry factor of 38.67 m^{-1} was reported by Vázquez *et al.* [14].

The theoretical bioelectrochemical consumption of acetate was calculated based on Faraday's Law from the coulomb exchange between each time interval (Eq. 1), multiplied by the molecular weight of acetate (59 g mol^{-1}), divided by the number of electrons liberated from the acetate oxidation (8) and divided by the Faraday constant (96 485 C mol^{-1} [37]), as reported in Eq. 3.

$$Consumed\ acetate(g) = \frac{C\ (coulombs) * 59\ \left(\frac{g}{moi}\right)}{8 * 96485\ \left(\frac{coulombs}{mol}\right)} \tag{3}$$

A summary of the experimental procedure is reported in Fig. 1-A. For the first 10 days, the BGRs were operated in batch mode in the anode medium. On day 9, before performing the polarization curve, the BGRs were fed with 1 mL of lactate 60% in water, to prevent possible bias due

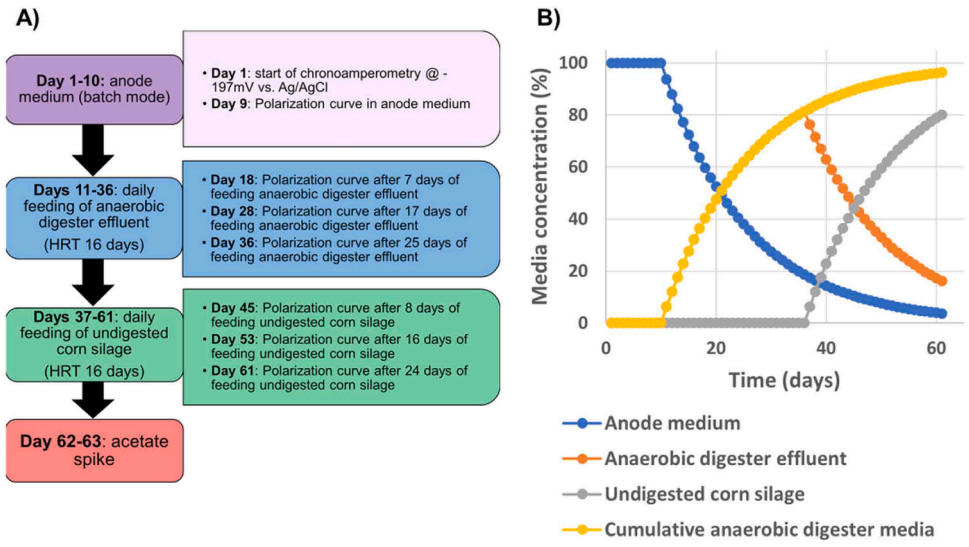

Fig. 1. A: experimental operation diagram. B: evolution of the media concentration in time during the experimentation. The cumulative anaerobic digester media is the sum of the anaerobic digester effluent concentration and the undigested corn silage concentration.

to substrate limitation. From day 11 to day 36, the BGRs were operated in fill-and-draw mode, feeding ADE at an OLR of 1.44 $gO_2\ L_{reactor}^{-1}\ d^{-1}$. The daily feeding amount corresponded to 6.25% of the 960 mL reactor volume, for a hydraulic retention time of 16 days. Polarization curves were recorded on days 18, 28, and 36. From day 37 to day 61 the feeding substrate was changed to undigested corn silage at an OLR of 3.31 $gO_2\ L_{reactor}^{-1}\ d^{-1}$. The polarization curves were recorded on days 45, 53, and 61. On day 62 and day 63, the BGRs were spiked with 60 mL of an 8 $g\ L^{-1}$ sodium acetate solution. All the media were fed without prior anaerobization to the BGRs. The daily analysis of pH, conductivity, soluble chemical oxygen demand, and organic acid concentrations were performed always before the daily feeding event. Fig. 1-B reports the evolution of concentrations of all the media during the experiments due to media exchange. It is worth noticing that this only gives an indicative representation of the evolution of the BGRs liquid phase composition: it is safe to assume that the microorganisms contained in the ADE proliferated in the anode medium, bringing a dynamic evolution of the biological and chemical composition of the BGRs liquid phase which could have established anaerobic digester conditions faster than the only exchange of media. However, following this experimental procedure, it is possible to study the evolution of the current densities of the different materials during the stepwise adaptation to anaerobic digester conditions, and afterward to investigate the change in current densities determined by the stepwise addition of an undigested media. While the ADE has a total COD of 23 $gO_2\ L^{-1}$ composed mostly of microbial biomass and hardly degradable substrates, the undigested corn silage has a total COD of 53 $gO_2\ L^{-1}$ and, since the solid silage was autoclaved and kept frozen until further use, the number of living microorganisms in it should be minimal, and most of the COD being composed of readily biodegradable substrates.

2.6. Corrosion experiments

Metallic materials are susceptible to corrosion when operated as anodes. In our experiments, stainless steel wool achieved the highest current densities in almost all conditions, while the other two metallic materials (stainless steel mesh and stainless steel plate) achieved only negligible current densities when operating with ADE and undigested corn silage. To rule out the possible contribution of abiotic corrosion to the current densities achieved by stainless steel wool, we investigated its possible corrosion following the methodology described by Vázquez *et al.* [14].

Linear sweep voltammetries (LSV) were carried out between −550 mV vs. Ag/AgCl and 550 mV vs. Ag/AgCl at a scan rate of 1 $mV\ s^{-1}$ in a three-electrode set-up inside modified Schott bottles. The previously mentioned platinized titanium mesh was also used as the counter electrode. The LSV were carried out in independent triplicates under continuous purging with a CO_2/N_2 gas mixture in anode media, anaerobic digester effluent and undigested silage. The LSV were carried out both in biological conditions (denominated "raw media") and in autoclaved media. The experiments in autoclaved media were conducted to rule out possible contributions from electroactive microorganisms to the assessed corrosion current densities. The anode media is expected to be abiotic, but it was nevertheless investigated in both conditions for comparison. The media were autoclaved at 121 °C for 20 min. The autoclaving process not only determines the death of all living cells in the media but also causes a change in the media pH, buffer capacity, and chemical composition, due to the possible thermal degradation of organic compounds. However, autoclaving is one of the easiest and most efficient sterilization methods, and other methods (e.g., addition of chemicals, filtration) would determine even bigger changes in the media conditions, without granting the same sterilization efficiency.

The corrosion was assessed based on the corrosion potential and the calculated exchange current density in the Tafel plot. Furthermore, abiotic chronoamperometry at −197 mV vs Ag/AgCl were carried out for 7 days under continuous purging with a CO_2/N_2 gas mixture, followed by polarization curves. The experimentation was carried out in independent duplicates for the three autoclaved media in a three-electrode set-up inside modified Schott bottles.

2.7. Metagenomic analysis

For the metagenomic analysis of the different electrode materials, the bioanodes were harvested after the experiment and stored in about 20 mL Allprotect Tissue Reagent (Qiagen, Hilden, Germany) at −20 °C until further processing. To extract the genomic DNA, a 2 cm^2 piece of the bioanodes was cut out and the DNA was then directly isolated using the Qiagen DNeasy PowerBiofilm kit (Qiagen, Hilden, Germany) according to the manufacturer's instructions. The total concentration and purity of the extracted DNA was measured using a NanoDrop 2000 spectrophotometer (Thermo Scientific, Waltham, MA, USA) and the Qubit dsDNA assay kit (Life Technologies, Carlsbad, CA, USA). Samples were stored at −20 °C until metagenome sequencing. A total of 400 ng

Qubit double-stranded DNA per sample was used for library preparation using the Native Barcoding Kit 24 V14, SQK-NBD114.24 (Oxford Nanopore Technologies, Oxford, UK). Sequencing was performed using a MinION Mk1b and an R10.4.1 flow cell with MinKNOW software v.22.10.7 (Oxford Nanopore Technologies, Oxford, UK). Base calling and demultiplexing were performed using Guppy v.6.4.2 in super accuracy mode with read splitting enabled and a minimum score of 58. Read assembly was performed using Flye v.2.9.1.-b1768 with the additional parameters -nano-hg and -meta. The contigs were then polished twice using Racon v.1.5.0 and once using Medaka v.1.8, model r1041 e82 400 bps sup g615. Minimap2 v.2.24 was used for read mapping. Polished contigs were annotated using the GTDB-tk v2.1.1 with database r207 v2. Coverage of contigs was assessed using Minimap2 and Samtools v1.16.1. For taxonomic representation, values for the same order were cumulated.

3. Results and discussion

3.1. Chronoamperometry

Fig. 2 shows the current densities for the 6 electrodes in the two different reactors. During the first experimental block (corresponding to the first 10 days of batch operation in anode medium), the reactor inoculated with a co-culture of *G. sulfurreducens* and *S. oneidensis* (BGR-GS) showed a clear hierarchy of materials, with stainless steel wool (SSW) being the best-performing material. Carbon nanofibers ES300 (CNF-ES300) performed similarly to graphite plate (GP) while stainless steel mesh (SSM) and graphite felt (Felt) performed similarly between them. Stainless steel plate (SSP) showed the lowest performance of the set. SSW was the best-performing material also in the case of the reactor inoculated with the natural microbial consortium (BGR-NMC); at the same time GP, CNF-ES300, and Felt performed similarly between them, while SSM and SSP did not show appreciable current production throughout the entire experimentation. During this first experimental block, in BGR-GS all electrodes started their current production in less than 2 h after the start of the chronoamperometry and exhibited a general decreasing trend in current densities after the first current density peak. In BGR-NMC the current production started after 2 days and all the electrodes showed an overall increasing trend in the current production. These differences were probably due to the different inoculation procedures of the two BGRs. However, both BGRs showed similar current densities for SSW, Felt, CNF-ES300 and GP in these conditions between days 5 and 10.

In the second (days 11–36, ADE as feeding substrate) and third (days 37–61, undigested corn silage as feeding substrate) experimental blocks, the BGRs were operated in fill-and-draw mode, with a daily feeding amount corresponding to 6.25% of the reactor volume and a hydraulic retention time of 16 days. Undigested corn silage becomes ADE after being fermented for 40 days in a lab-scale anaerobic digester; therefore, the main difference between the two media is the biodegradation level. Upon the start of ADE addition on day 11 and in the entire second block, all the electrodes in both BGRs presented a stepwise decrease in current production. Around day 23, all materials in both BGRs started displaying a trend characterized by current peaks immediately after each feeding event, followed by a sharp decline. This trend stayed consistent for the remaining duration of the second experimental block. For instance, for SSW in BGR-GS, on day 35 the current peaked 3.84 h after the feeding event, with a current density going from 0.04 mA cm^{-2} to 0.22 mA cm^{-2} (5-fold increase) and then slowly decreased to 0.07 mA cm^{-2} at day 36, right before the next feeding event. This is in agreement with Kretzschmar *et al.* [23] who also reported current density peaks in correspondence to feeding events, correlating this effect to an acetate concentration peak reached immediately after the feeding event and a subsequent decrease of the acetate level until the next feeding event [23]. In this same study, bioanodes derived from a *Geobacter anodireducens*-dominated secondary biofilm on graphite rods showed a similar deactivation trend as the one reported in the second experimental block of our experiments, going from a peak current density in the range of 0.17 mA cm^{-2} during the first day of operation inside an anaerobic digester to a peak current density of less than 0.03 mA cm^{-2} after 8 days of operation [23]. For comparison, GP (the electrode material of the present study which is the most similar to graphite rods used by Kretschmar *et al.*) in BGR-GS even towards the end of the ADE addition phase still reached current density peaks in the range of 0.1 mA cm^{-2}, while GP in BGR-NMC stopped performing on day 13 going from 0.23 mA cm^{-2} to 0.02 mA cm^{-2}, and did not show any change during the rest of the experimentation. During the second experimental block, in BGR-GS could still be observed a ranking of materials, with SSW being the best-performing material in the entire second block, followed by CNF-ES300 and Felt which performed similarly. On average, SSW peaks reached double the maximum current densities of CNF-ES300 and Felt. The picture changed in BGR-NMC: CNF-ES300 and Felt were the two best materials, with similar performances, and SSW ranked in third position.

Immediately after the first addition of undigested corn silage in the third experimental block, in BGR-GS the current densities peaks for SSW, CNF-ES300, and Felt doubled. Thus, SSW went from a maximum peak of 0.16 mA cm^{-2} to a maximum peak of 0.32 mA cm^{-2}. In this phase, it was also possible to observe more stable current densities for all the electrode materials and a clear ranking of them, with SSW being the best-performing material, followed by CNF-ES300, Felt, GP, SSM, and SSP. The addition of undigested corn silage also improved the current densities generated by the porous electrodes in BGR-NMC, while the flat materials did not show any improvement from the change of feeding substrate. The current stabilized at around 0.2–0.3 mA cm^{-2} for SSW, Felt and CNF-ES300, which showed similar performances, while SSP, GP and SSM kept producing only negligible current densities.

For the last 2 days, the BGRs were spiked with acetate instead of feeding undigested corn silage, to test if increases in acetate concentration in the media would have caused a spike in current densities in the bioanodes. The calculated acetate concentration increases in the BGRs due to these spikes was 500 mg L^{-1}. On the other hand, the calculate acetate increase in the BGRs due to the undigested silage feeding (with an average concentration of acetate of 650 mg L^{-1}) was 40.6 mg L^{-1}, 12-times lower increase compared to the acetate spike. After the acetate spikes it was possible to notice a local spike in current, similar to the one observable after the ADE and undigested silage feeding events. However, no major current increase compared to the other two feeding substrates was observed, probably due to a fast consumption of acetate from the bulk microbes [38–40]. It is also possible to notice an overall decreasing trend of the current densities during the acetate spikes, compared to the plateau observed during the undigested silage feeding.

Fig. 3 displays the iR-corrected electrode potentials obtained during the chronoamperometry experiments reported in Fig. 2. Due to the uncompensated resistance caused by the low conductivity of the medium and the distance between the reference electrode and the working electrodes in the BGRs [36], the real potentials of the electrodes were more negative than the −197 mV vs Ag/AgCl setpoint of the potentiostat. The obtained results were in line with what was obtained from Vázquez *et al.* [14] with the same reactor geometry. Due to this effect, it is difficult to compare the current densities obtained throughout the experimentation from the different bioanodes [36], since all of them were polarized to different potentials, and those potentials changed dynamically during the entire experimentation. Polarization curves were performed to better clarify this point.

3.2. Polarization curves

Fig. 4 reports the maximum current densities obtained in the polarization curves, the minimum slope in the ohmic region of the polarization curves, and the cumulative charge exchanged in the two days prior and two days after each polarization curve. The complete iR-

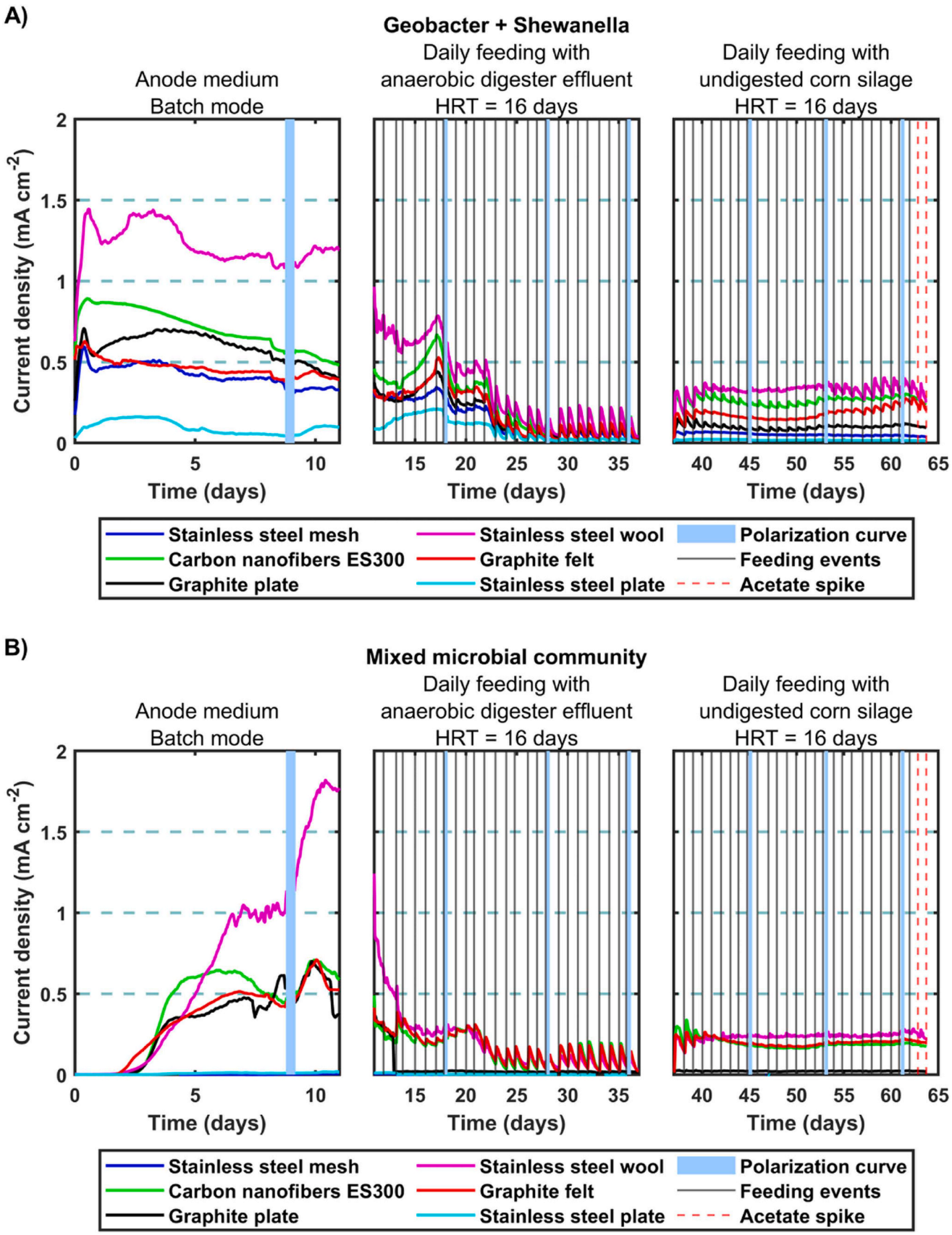

Fig. 2. Current densities for the 6 electrodes in the two different reactors (A, inoculated with a co-culture of Geobacter sulfurreducens and Shewanella oneidensis, and B, inoculated with a natural mixed microbial community from a lab-scale anaerobic digester). The daily feeding amount and acetate spikes correspond to 6.25% of the reactor volume. HRT: hydraulic retention time.

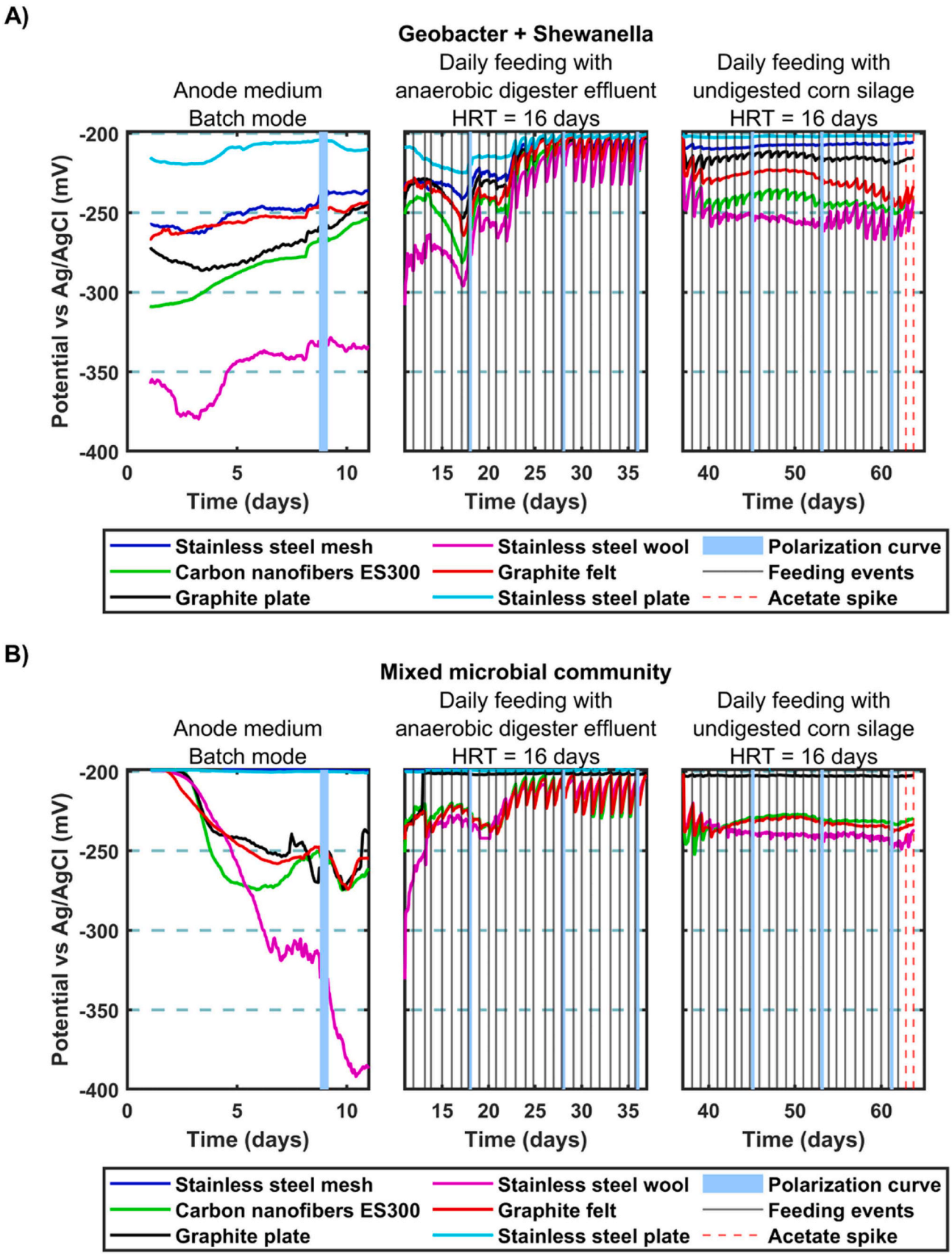

Fig. 3. A) iR-corrected electrode potentials for chronoamperometry in Fig. 1-A. B) iR-corrected electrode potentials for chronoamperometry in Fig. 1-B. HRT: hydraulic retention time.

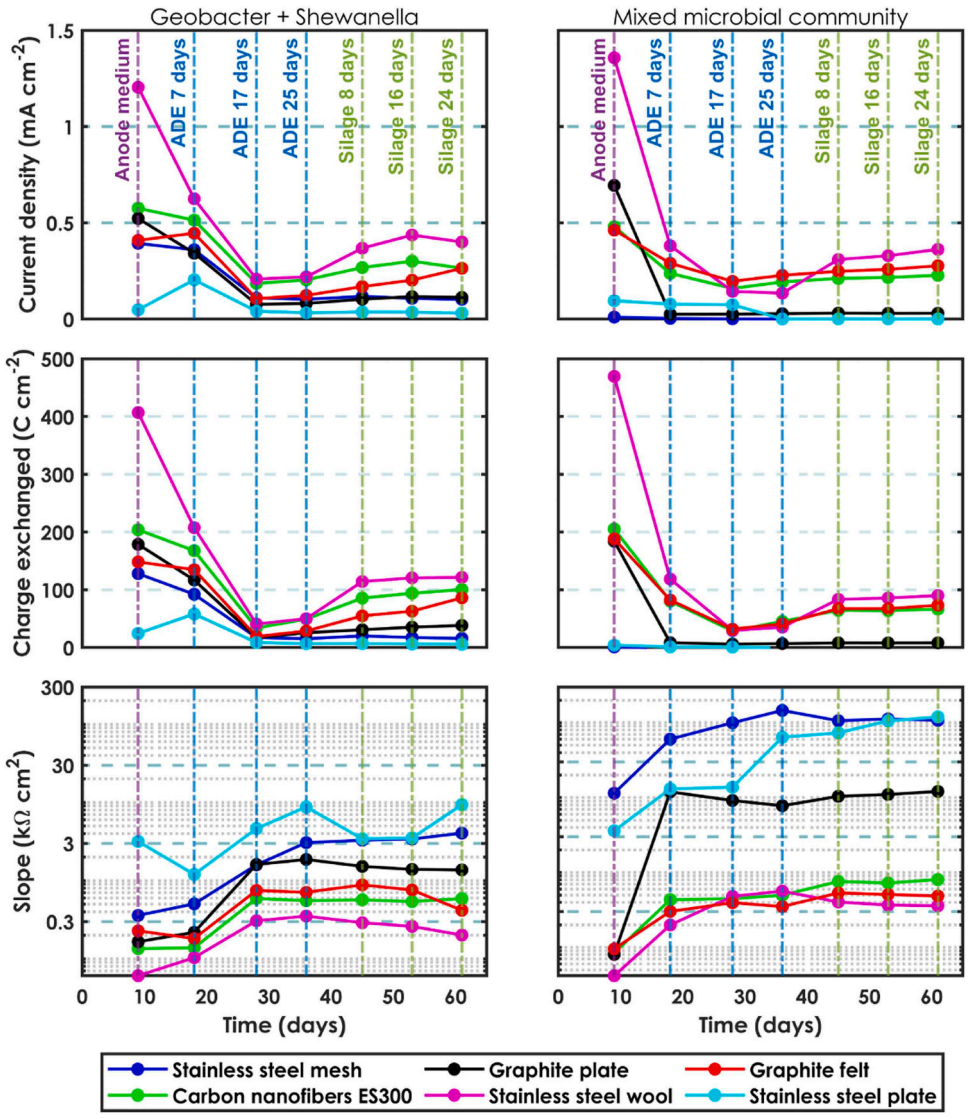

Fig. 4. From top to bottom: maximum current densities obtained in the polarization curves, cumulative charge exchanged in the two days prior and two days after each polarization curve, minimum slope of the ohmic region obtained in the polarization curves. The left column shows the results for BGR-GS, while the right column shows the results obtained in the case of BGR-NMC.

corrected polarization curves are reported in Figure S1 and Figure S2. In both BGRs the maximum current densities in anode media were in line with values reported in the literature for similar bioanodes. The maximum current densities in anode medium for Felt and SSM in BGR-GS were around 0.4 mA cm^{-2} for both materials, while Kipf *et al.* [17] reported maximum current densities of around 0.7 mA cm^{-2} for similar electrode materials operated as bioanodes in a similar anode medium with a pure culture of *G. sulfurreducens* (OD_{600} = 0.1) as inoculum. It is also worth noticing the outstanding current density (higher than 1 mA cm^{-2}) obtained by SSW in the anode medium, regardless of the inoculation procedure. The addition of ADE caused decreases of similar magnitudes in the maximum current densities and the charge exchanged for all materials in both BGRs. For instance, the maximum current density of GP in BGR-GS decreased from 0.5 mA cm^{-2} in the anode medium to 0.08 mA cm^{-2} after 17 days of ADE addition. On the other hand, SSW and CNF-ES300 reached, in both BGRs, maximum current densities in the range of 0.2 mA cm^{-2} after 17–25 days of ADE addition, when the ADE concentration in the liquid phase of the BGRs was between 36% (on day 17) and 62% (on day 25). For comparison, Dzofou Ngoumelah *et al.* [24] reported the operation of a 3-week-old *Geobacter spp.* EABf on graphite rods at different ADE concentrations. The maximum current densities produced by those bioanodes dropped below 0.1 mA cm^{-2} after 1 week of operation at ADE concentrations between 25% and 75%.

SSW in BGR-NMC achieved lower maximum current densities during ADE addition than Felt and CNF-ES300, while the charge exchanged in the 4-day interval around the polarization curve is about the same values for the three materials. This effect may be due to a combination of different causes. For instance, this effect could be related to the different mass transfer in the biofilm, which regulates the access to substrate, for the different electrode materials [41–43]. It is also important to notice how the maximum current densities are achieved in the polarization curves at set bioanode potentials, while the charge exchanged is calculated during the chronoamperometric control of the bioanodes. As shown in Fig. 3, the bioanodes potentials during the chronoamperometry change dynamically due to uncompensated resistance. Therefore, it may be possible that even if Felt and CNF-ES300 can achieve higher maximum current densities at more positive bioanode potentials, this doesn't reflect in an improvement of bioanodes performance in the middle-long term during chronoamperometric control. These results indicate how is important to not only consider maximum current densities when comparing bioanode performances

but also take into consideration the current densities trends and the related charge exchanged. The addition of undigested corn silage had little effect on the performances of the flat electrodes (SSM, SSP, and GP) while the porous ones showed a recovery in current densities and charge exchanged, even though not fully recovering to the performances obtained in the anode medium. It is worth noticing how the maximum current densities obtained by SSW, Felt, and GP in BGR-GS after the beginning of the addition of undigested corn silage are in the same range as the results presented for the same electrodes in the same type of reactor by Vázquez *et al.* [14] after 3 weeks of operation of the bioanodes (inoculated with real wastewater and *G. sulfurreducens*) in synthetic non-axenic brewery wastewater. Furthermore, the PC slopes reported in the same work for the aforementioned bioanodes are in the same range as the ones reported in our work for the same electrode materials in BGR-GS. The stepwise addition of ADE also determined an increase in the slope of all the electrodes in both BGRs. For instance, in both BGRs, SSW went from ~0.05 kΩ cm^2 in anode medium to ~0.3 kΩ cm^2 after 17 days of ADE addition. This effect may derive from the colonization of the EABf by fermenters and other non-electroactive microorganisms. These microbes form the biofilm structure by producing extracellular polymeric substances (EPS), a sort of "microbial glue" which keeps together the biofilm [44,45]. The increase amount of EPS and non-electroactive microbes could determine an increase in the EABf internal resistance [46,47]. The porous electrodes presented similar slopes in both BGRs, which stabilized at around 0.3–0.8 kΩ cm^2 from the beginning of ADE addition. On the other hand, the flat electrodes in BGR-NMC presented slope values 10–20 folds higher than their counterparts in BGR-GS.

In general, it is possible to observe how the maximum current densities obtained in the polarization curves and the charge exchanged in the selected timeframes for the two BGRs further validated the ranking (for BGR-GS) and grouping (for BGR-NMC) of materials obtained in the chronoamperometry, with SSW being the overall best-performing material. From our results, it can be noticed how the bioanodes that presented the lowest slope of the PC in the ohmic region, which indicates the internal resistance of the bioanodes, were also the best-performing ones in terms of maximum current densities in the PC and charge exchanged in the selected timeframes.

3.3. Corrosion analysis

SSW outperformed the other metallic materials in all our experimental conditions. For this reason, the corrosion tests were performed only on SSW, using LSV to evaluate the corrosion potentials and the corrosion current densities and quantify the possible contribution to the current densities achieved due to the corrosion of the material. The resulting Tafel plots are reported in Fig. 5, while the calculated corrosion potentials and corrosion current densities for all media and conditions are reported in Table S4.

The results for the LSV performed in the raw mediums (non-autoclaved and without any pre-treatment) showed that the corrosion current densities obtained were negligible compared to the current densities achieved in the biotic chronoamperometry. It is also possible that the obtained corrosion current densities were the result of the electrochemical oxidation of organic molecules on the electrode, or from the contribution of electroactive microorganisms. To discard this last hypothesis, we performed the LSV in autoclaved mediums to obtain results in strictly abiotic conditions. The obtained corrosion current densities (Table S4) in autoclaved mediums were around 1 order of magnitude lower than the ones obtained in the raw mediums.

To obtain a comparison with the results reported in the previous experimental sections, SSW was polarized at the −197 mv Vs Ag/AgCl (same potential of the chronoamperometry) over 7 days in duplicate in the three media. The media were autoclaved to prevent the formation of an electroactive biofilm. After 7 days, PC were recorded in the same way as previously described. The resulting PCs are reported in Figure S3. The current densities obtained were negligible compared to the results from the biotic chronoamperometry and polarization curves reported in the previous Sections.

In conclusion, from the results achieved in the corrosion experiments, it is possible to claim that the outstanding electrochemical performances of the SSW bioanodes were due to pure bioelectrochemical activity, with minimal contribution due to material corrosion, in agreement with precedent literature [14].

3.4. Battery glass reactors conditions

The bioreactor parameters (pH, conductivity, and soluble COD) through the experimentation are reported in Fig. 6. It is worth

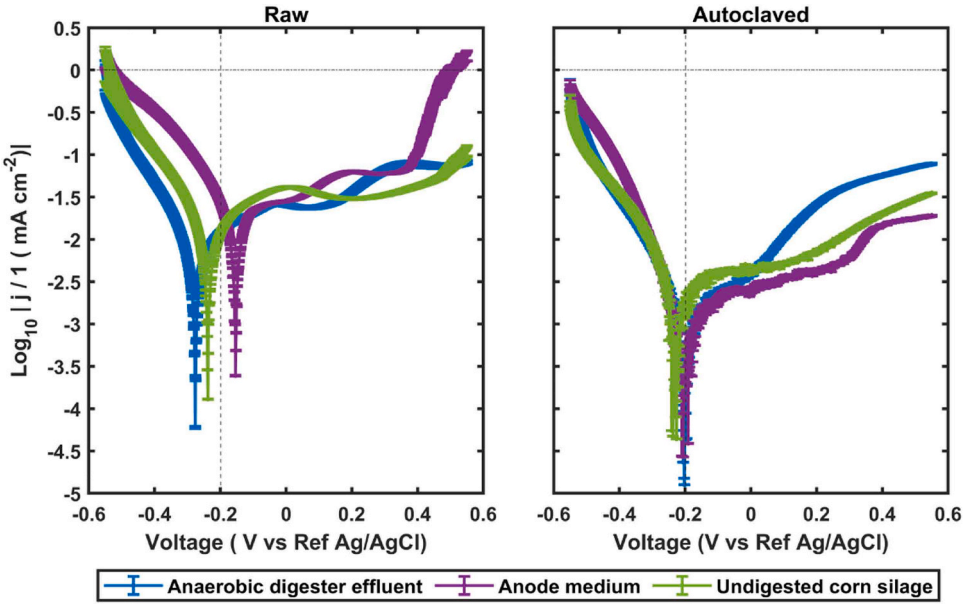

Fig. 5. Tafel plots for the three different media (anaerobic digester effluent, anode medium, and undigested corn silage) in the two different conditions (raw and autoclaved). The LSV were conducted between −550 mV vs. Ag/AgCl and 550 mV vs. Ag/AgCl at a scan rate of 1 mV s^{-1}.

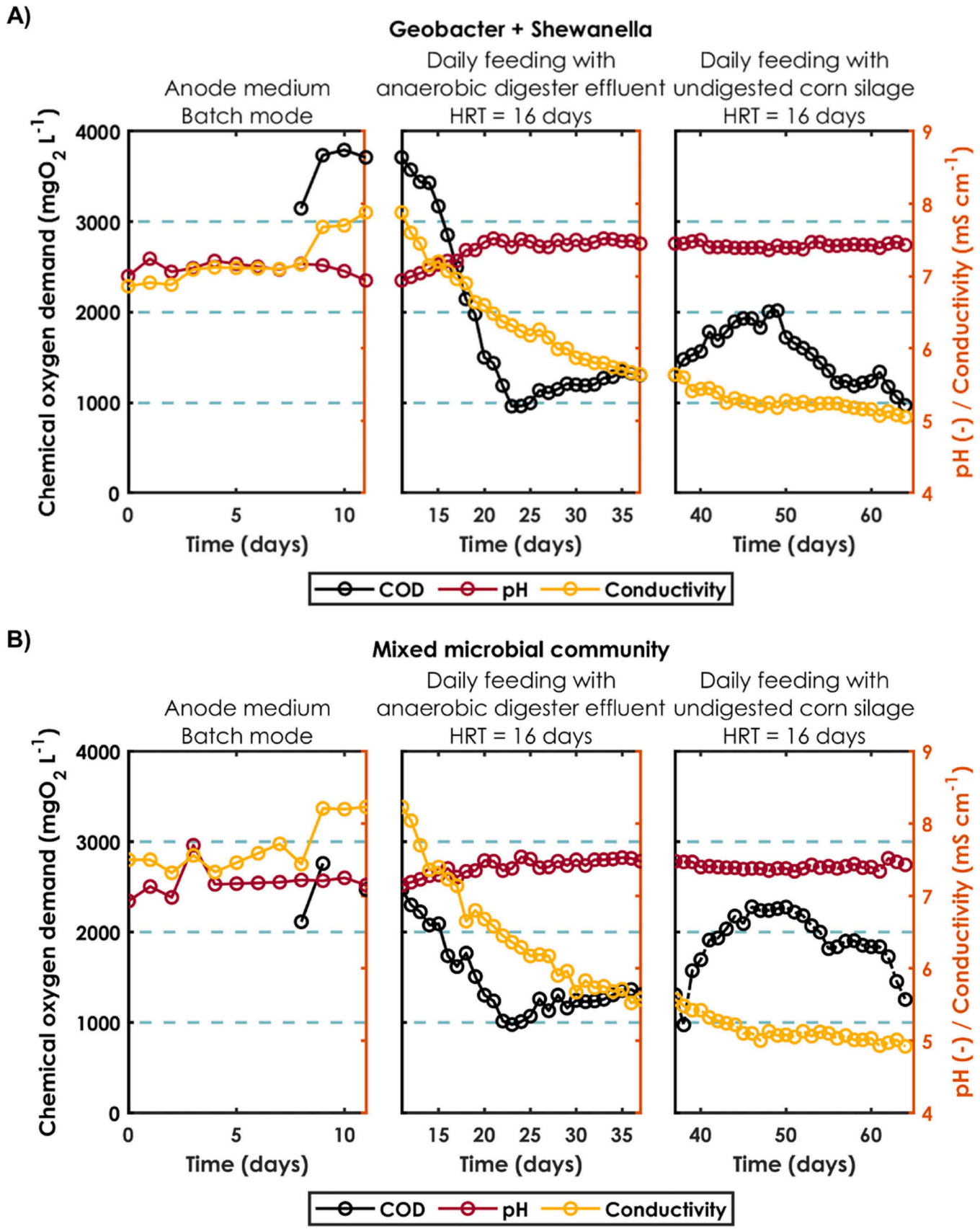

Fig. 6. Evolution of soluble COD, pH, and conductivity for the two BGRs. (A, inoculated with a co-culture of Geobacter sulfurreducens and Shewanella oneidensis, and B, inoculated with a natural mixed microbial community from a lab-scale anaerobic digester). The analyses were done immediately before the feeding events. HRT: hydraulic retention time.

mentioning that in the second and third experimental blocks, the samplings for the analysis were carried out always before the daily feeding event, therefore, the presented values describe the BGRs' conditions when the substrates were depleted after 24 h of microbial activity. The feeding events may have caused changes in the BGRs' conditions during the 24 h between each analysis.

The pH remained constant at around 7.5 for both BGRs, possibly due to the high buffer capacity of the media utilized in these experimentations and the continuous gas purging with 20% CO_2, which kept constant the gas composition on the BGRs' headspace and stabilized the carbonate buffer. A neutral pH of around 7–7.5 is considered the optimum for methanogenesis and AD processes [48,49], however, more alkaline pHs are considered beneficial for the electrochemical response of bioanodes [50,51]. Accordingly, a pH of 7.5 could be considered the optimum "middle-point" to benefit both the AD microbial community and the bioanode EABf. Since the pH trends of both BGRs has been exactly the same for the entire duration of the experimentation (except for an outlier for BGR-NMC at day 3), an influence of the pH on the different electrochemical response of the BGRs can be ruled out.

The conductivity decreased for both BGRs from the start of the addition of ADE and reached a plateau at around 5 mS cm^{-1}. This is due to the addition of a media with lower conductivity (ADE and undigested corn silage, both with a conductivity of ~ 4–5 mS cm^{-1}) to the anode medium, which instead had a conductivity of ~ 7–7.5 mS cm^{-1}. The soluble COD showed an increase in day 9, due to the lactate addition, then rapidly decreased for both BGRs from the beginning of ADE feeding. This could be explained by the fact that the ADE contained a microbial community of fermenters and methanogens which can rapidly biodegrade COD [52,53]. On the other hand, the COD showed an increasing trend after the beginning of undigested corn silage addition. This could be due to the difference in biodegradability between the two media. The higher amount of biodegradable substrate in undigested corn silage could also have stimulated the microbial activity in the bulk of the BGRs, explaining the latter decrease in COD from day 50.

Fig. 7 describes the profiles through time for the concentrations of acetic acid, propionic acid, butyric acid, and lactic acid. The HPLC analyses were carried out on the same sample utilized for the COD, pH and conductivity analysis, consequently the sampling for the analysis in the second and third experimental blocks was carried out always before the daily feeding event. Consequently, the organic acids concentrations describe the BGRs' conditions when the substrates were consumed by 24 h of microbial activity. For comparison, in Figures S5 and S6 are reported, respectively, the organic acids profiles of ADE and undigested corn silage.

In the first experimental block, lactic acid, which was the only substrate initially added and present with a starting concentration of 3.73 g L^{-1}, was present in only a minimal amount until day 9. This may be due to its fast consumption by *S. oneidensis* in the bulk phase of BGR-GS and by the fermenters present in the inoculum of BGR-NMC [54]. The biodegradation of lactic acid and yeast extract, present in a concentration of 1 g L^{-1} in the anode medium, determined the relatively high concentrations of acetic acid and propionic acid detected in the anode medium [55]. Three moles of lactate can be fermented to two moles of propionate and one mole of acetate [55]. Accordingly, the complete fermentation of the 3.73 g L^{-1} of lactate present at the beginning of the experiment would result in a propionate concentration of 2 g L^{-1} and an acetate concentration of 0.8 g L^{-1}, which is in line with the detected concentrations of such compounds. Acetic acid was always present in concentrations above 400 mg L^{-1} in both BGRs during the first experimental block. However, the two BGRs presented different acetic acid trends until day 9: increasing for BGR-GS and decreasing for BGR-NMC. The increase of acetate concentration in BGR-GS could be due to the fermentation of yeast extract, while the decreasing trend of acetate in BGR-NMC could be due to the presence of acetate-consuming microbes in the inoculum [35]. The concentration of propionic acid during the first experimental period was high and stable and without major changes for both BGRs, around 1000 mg L^{-1} for BGR-GS and around 800 mg L^{-1} for BGR-NMC. The propionate may have been produced by ubiquitarian fermenters present in the environment [56], which proliferated in the anode medium and fermented the lactate to propionate. The butyric acid concentration was minimal in both BGRs for the entire duration of the experimentation and without significant changes. The addition of lactate on day 9, before the analysis, determined an increase in the concentrations of acetic acid and propionic acid in both BGRs, in agreement with the hypothesis that these organic compounds are produced by fast biodegradation of lactate. Acetic acid then decreased rapidly in BGR-NMC, while it kept increasing in BGR-GS. During the entire experimentation, the total daily bioelectrochemical consumption of acetate (sum of acetate consumed by all the six bioanodes inserted in the BGR) has been in the 5–60 mg day^{-1} range for both BGRs. The total daily theoretical bioelectrochemical consumption of acetate by the bioanodes during the entire experimentations are reported in Figure S4. In relation to this, the reduction of acetate concentration due to its bioelectrochemical oxidation at the bioanodes is minimal in comparison to the acetate levels in the BGRs. The decrease of the acetate concentration in BGR-NMC can thus be explained by the presence of acetate-consuming microbes in the inoculum utilized [35].

In the second block, the acetic acid concentration of BGR-GS started to decrease due to the addition of ADE, which contained acetate-consuming methanogens and had an average acetate concentration of 470 mg L^{-1} and stabilized around a value of 600 mg L^{-1} from day 20. BGR-NMC showed a decreasing trend similar to the previous block, which then changed to an increasing trend from day 19 and stabilized at a value of 600 mg L^{-1}. In both BGRs, propionic acid showed a decreasing trend from the start of ADE addition and stabilized at around day 22 to a value of 100 mg L^{-1}. The inoculum utilized for BGR-NMC should contain propionate-consuming microbes [57], but, since no propionate degradation was present in the first experimental phase, it would be possible to hypothesize that the anode medium conditions did not allow the propionate-consuming microorganism to prosper. The beginning of ADE addition increased the amount of propionate-consuming microorganisms present in the BGRs [57], determining a fast propionate consumption.

In the third block, in both BGRs, acetic acid increased after the beginning of the addition of undigested corn silage, then started to show a decreasing trend. The last 2 days of acetate spikes did not determine an increase in the measured acetic acid concentrations. This effect can be explained by the fast consumption of acetate by the organisms present in the planktonic phase [52,53,58]. The propionic acid amount was higher in BGR-NMC than in BGR-GS and did not decrease as sharply, but in both cases, it showed a trend similar to the acetic acid one. Propionate also showed a rapid decrease in BGR-NMC during the acetate spike since no further propionate is added during the acetate spike and the propionate consuming microbes rapidly metabolized the propionate accumulated in bulk during the undigested silage feeding. Also lactic acid showed a similar trend in both BGRs, with a decreasing trend compared to the second block. These differences could be due to the intrinsic heterogeneity of the independent BGRs.

In general, it is worth noticing how the BGRs could operate at an HRT of 16 days while being fed with undigested corn silage at an OLR of 3.31 gO_2 L^{-1} day^{-1} without presenting any sign of overacidification. This OLR is 2.5-folds higher than the OLR of the laboratory scale anaerobic digester fed with undigested corn silage and operated to obtain the ADE. For comparison, the lab-scale AD presented signs of overacidification and process inhibition for HRT lower than 40 days (data not showed). During the 24 days of operation in these conditions, the BGRs did not present any pH decrease nor soluble COD or organic acids accumulation. During the third experimental phase (undigested corn silage feeding), the total daily bioelectrochemical consumption of acetate was in the 10–20 mg day^{-1} range. From these results it is possible to hypothesize that the bioanodes can improve the anaerobic digestion process stability even if the amount of acetate degraded by the bioanodes is very low

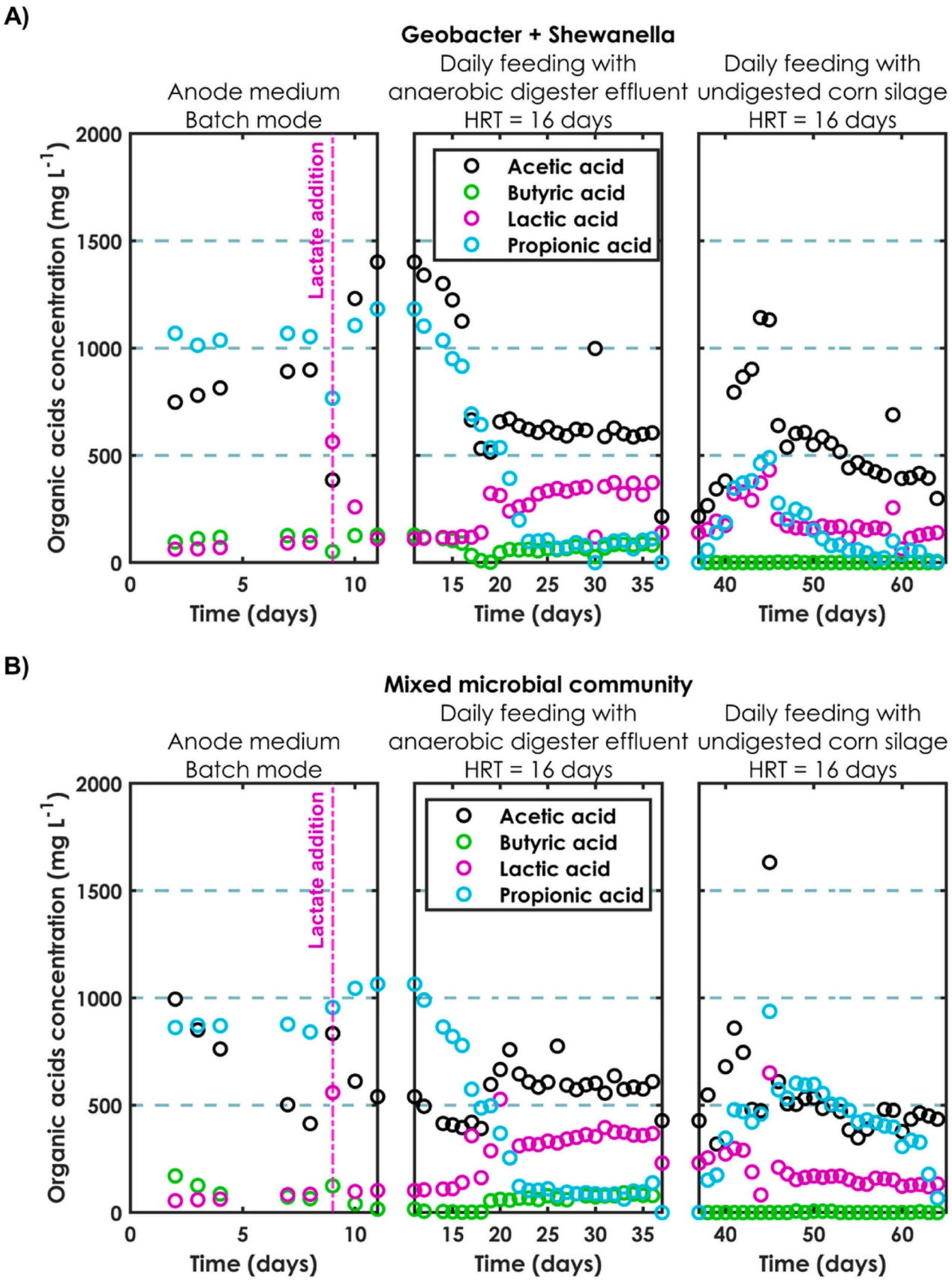

Fig. 7. Organic acids concentrations over time for the two BGRs (A, inoculated with a co-culture of Geobacter sulfurreducens and Shewanella oneidensis, and B, inoculated with a natural mixed microbial community from a lab-scale anaerobic digester). The analyses were done immediately before the feeding events. HRT: hydraulic retention time.

compared to the OLR of 3.31 gO_2 L^{-1} day^{-1} during the third experimental phase.

3.5. Bioanalysis

To gain insight into the microbial community colonizing the two best-performing electrode materials, SSW and CNF-ES300, a metagenomic analysis was performed on them. Fig. 8 shows the orders with an abundance greater than 1% in at least one of the samples, which were defined as major contributors, while all classified microbial genera are provided in the Table S5. A total of 15 major contributors were identified, with Geobacterales being the most abundant order in all four samples. The only species that was found within the order of Geobacterales was *G. sulfurreducens* (Table S5). The abundance of this species was higher on the CNF electrodes with 38% for BGR-GS and 33% for BGR-NMC compared to the SSW electrode with 30% and 27% for BGR-GS and BGR-NMC, respectively. *Geobacter* species are reported to be the most common exoelectrogens in MEC-AD processes with relative abundances of up to 70% [59–61], so the abundances found on all four bioanodes are consistent with the literature. Pre-cultivation of *G. sulfurreducens* and *S. oneidensis* resulted in a higher abundance of *G. sulfurreducens* for both electrodes compared to the system inoculated with natural mixed microbial community, but the difference found was relatively small with 5% and 3% higher abundance for the CNF and SSW electrodes, respectively. Interestingly, *S. oneidensis* could not be identified at all (Table S5) on any of the anodes analyzed. This indicates that *S. oneidensis* could not be established as part of the anode biofilm. In the study of Liu *et al.* [61] a similar effect was reported, where a pre-cultivated MEC-anode was introduced into an anaerobic digestion reactor and *Shewanella* species were only detected after the start-up but not in the final analysis of the bioanode. In addition, Engel *et al.* [62] showed that *S. oneidensis* was not part of the established biofilm of an MEC-anode, but that the presence of this organism had beneficial effects on the current production of *G. sulfurreducens* that colonized the electrode material.

Besides Geobacterales, a high abundance of fermentative organisms was identified. In particular, species of the order Bacteroidales were found to dominate the SSW bioanode with 21% for the system with pre-cultivation and 22% for the system with the NMC. On the CNF bioanode, Bacteroidales were found with an abundance of 5% and 4% of the pre-cultivated and the NMC system, respectively. Species of this order are known for their high potential to degrade lignocellulosic substrates as well as amino acids into acetate and ammonia and their high abundance in AD processes was previously reported [63,64]. Furthermore, a high abundance of Petrotogales was found on the CNF bioanode with (1.2%) and without (1.3%) pre-cultivation as well as on the SSW bioanode with (5%) and without (8%) pre-cultivation. This order of bacteria is known to produce mostly acetate, and, in minor amount, propionate and succinate, fermentatively from lactate and glycerol in AD processes [65]. The ability of this order to produce acetate could explain the high abundance found on the bioanodes as it suggests a close interaction of these organisms with *G. sulfurreducens* cells which utilize acetate as their energy and electron source. Accordingly, Synergistales were found as major contributor on both CNF electrodes (up to 2%), while being a minor contributor on the SSW electrodes (<1%). This order was reported to be able to degrade several amino acids [64,66] and lactate [65] to produce acetate as well. Syntrophales were found as major contributor on the SSW electrode with pre-cultivation (1%), whereby these organisms are reported to contribute to the degradation of butyrate, iso-butyrate, and iso-valerate to produce acetic acid [67]. Additionally, Propionibacteriales were found with an abundance of around 1% on the SSW bioanode and with a slightly lesser abundance of around 0.9% for the pre-cultivated CNF bioanode and 0.1% for the CNF bioanode without pre-cultivation. These organisms are also known to contribute to AD processes mainly for their production of propionate [65].

In addition, several species of the phylum Firmicutes were identified on the tested bioanodes (Table S5). Firmicutes are syntrophic bacteria known to degrade volatile fatty acids (VFAs) to hydrogen and have been reported as key organisms for anaerobic digestion processes [68]. The hydrogen produced by these organisms in a conventional AD process is used by hydrogenotrophic methanogens to produce methane [68]. In the bioanodes studied here, it is also conceivable that *G. sulfurreducens* utilized the hydrogen produced locally by these organisms in the anode biome, as this organism can use hydrogen as an electron donor alongside acetate [69]. Consistent with this, an abundance of 0.1–2.7% of Cloacimonadales, an order also known for its interaction with hydrogenotrophic methanogens in AD processes [70,71], was found on all bioanodes. The syntrophic interaction with methanogens was further reported for organisms of the order Anaerolineales [72], which were

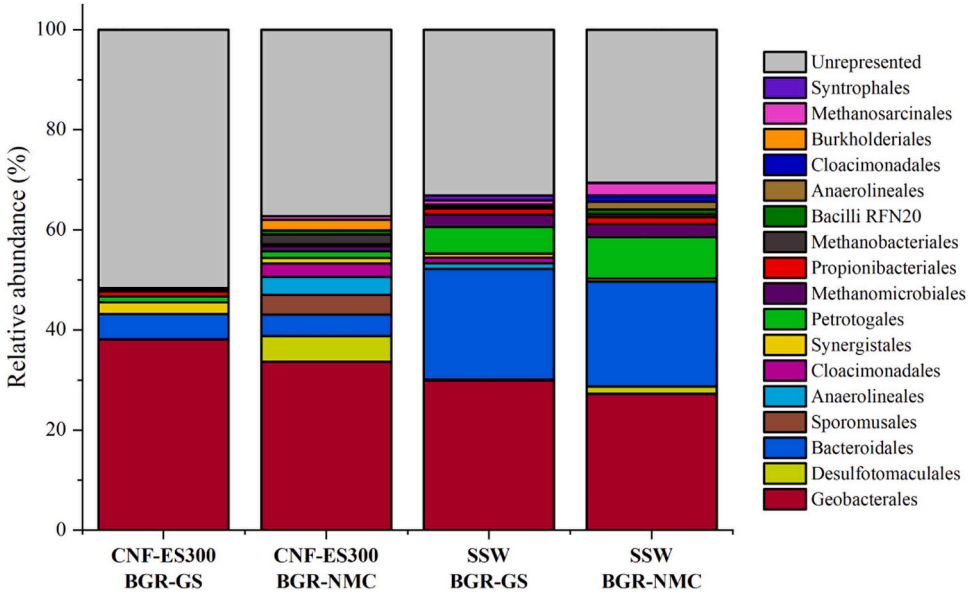

Fig. 8. Relative abundance (%) of microbial orders colonizing the bioanode. The microbial diversity on the two best-performing bioanodes (CNF and SSW) was analyzed using metagenome sequencing. Unclassified genera were excluded after the analysis. Orders with abundance >1% in at least one of the samples are given in the bar chart, while all classified genera are listed in Table S5.

found as major contributor with an abundance of 1% for both SSW electrodes and 3.5% for the CNF electrode with NMC. These organisms are known to utilize various substrates, such as sugars, peptides, and organic acids in the AD process [72]. Lastly, Burkholderiales, which were found only on the CNF electrode with NMC (2%), are reported to be involved in the production of VFA and hydrogen from more complex organic matter, including aromatic compounds [73,74].

As third group besides fermentative organisms and the exoelectrogenic organism *G. sulfurreducens*, a total abundance of methanogens with 0.5% and 3.7% for CNF and 3.8% and 5.6% for the SSW bioanode with and without pre-cultivation, respectively, were identified. Three different orders of methanogens were found, namely Methanobacteriales, Methanosarcinales, and Methanomicrobiales. While both Methanobacteriales and Methanomicrobiales are classified as hydrogenotrophic methanogens, Methanosarcinales can utilize acetate for the formation of methane [75,76]. Therefore, the presence of all three orders is in line with the other identified bacterial orders on the bioanode, as these groups provide hydrogen as well as acetate for the methanogens. However, an abundance below 6% of the methanogens compared to the 30% abundance found for *G. sulfurreducens* could imply that most of the produced acetate and hydrogen was utilized by the exoelectrogenic organism. Furthermore, *Geobacter* species were reported to be able to perform direct interspecies electron transfer (DIET) with electrotrophic microorganisms [77], suggesting a close interaction between *G. sulfurreducens* and the identified methanogens. This would directly influence the monitored current density, however, the low abundance of methanogens on the bioanode (<6%) might indicate that this interaction and the negative effect of DIET on the current production was rather limited.

In general, the microbial orders identified in the bioanalysis of the bioanodes correspond to the groups known in the literature to be involved in the AD process. Interestingly, the CNF anode, especially the one where the pre-cultivation of *G. sulfurreducens* and *S. oneidensis* took place, showed a higher abundance of unclassified or underrepresented orders compared to the SSW electrode. This implies that the CNF material provided an environment in which a more diverse biofilm could be established, whereas the SSW resulted in a more dominant presence of e.g. Bacteroidales and Petrotogales in the bioanode in comparison. Furthermore, the inoculation strategy did not affect the biodiversity in the bioanode of the SSW material, whereas a difference was found for the CNF electrode. Nevertheless, both electrode materials in which a pre-cultivation took place resulted in a slightly better performance in terms of current density (Fig. 2), which might indicate that the pre-cultivation has a beneficial effect on the performance of the bioanode regardless of the biodiversity found in the performed bioanalysis.

4. Conclusions

Geobacter-dominated bioanodes, using stainless steel wool and carbon nanofibers as base material, were successfully operated long-term under real anaerobic digester conditions. After 60 days of operation, these bioanodes achieved unprecedented stable current densities of 0.4 mA cm^{-2}, up to four times higher than previously reported values under similar conditions. Notably, porous electrodes, such as stainless steel wool and carbon nanofibers, consistently outperformed flat electrodes over the long-term, regardless the inoculation procedure and the fermentation grade of the substrate. Furthermore, as the blank experiments showed, the currents associated with the corrosion process for the stainless steel wool were negligible. The influence of the inoculum, whether a define mixed community of electroactive microorganisms or a natural mixed microbial community, on the performance achieved by the porous electrodes was minimal. By contrast, the microbial composition of the bioanodes depends mainly on electrode material rather than the inoculation procedure. Another significant factor that affecting the performance of porous electrodes was the biodegradability grade of the feeding media. Bioanodes from porous electrodes exhibited more than twice the current density when the reactors were fed with undigested corn silage instead of anaerobic digestor effluent, demonstrating the potential for direct integration of microbial electrolysis cells into anaerobic digesters without pre-fermentation steps. After establishing anaerobic digestion conditions, the reactors were operated at an HRT of 16 days, without over-acidification nor COD accumulation. Even though the calculated bioelectrochemical consumption of acetate was relatively low to play a major role in the COD removal, it can be hypothesized that the bioanodes had a beneficial effect on the anaerobic digestion process. These findings represent a step forward towards the development of bioanodes which can be utilized in real industrial applications.

CRediT authorship contribution statement

Simone Colantoni: Writing – review & editing, Writing – original draft, Visualization, Validation, Methodology, Investigation, Formal analysis, Data curation, Conceptualization. **Óscar Santiago:** Writing – review & editing, Supervision, Methodology, Conceptualization. **Janek R. Weiler:** Writing – review & editing, Investigation. **Melanie T. Knoll:** Writing – review & editing, Investigation. **Christian J. Lapp:** Writing – review & editing, Investigation. **Johannes Gescher:** Writing – review & editing, Resources, Project administration, Funding acquisition. **Sven Kerzenmacher:** Writing – review & editing, Supervision, Resources, Project administration, Funding acquisition, Conceptualization.

Declaration of Competing Interest

The authors declare that they have no known competing financial interests or personal relationships that could have appeared to influence the work reported in this paper.

Data availability

Data will be made available on request.

Acknowledgments

The authors gratefully thank the German Federal Ministry of Food and Agriculture (BMEL) for their financial support under the program “BiBER” (Grant No. 2219NR379). We thank Dr. Guillaume Pillot for fruitful discussions and critical feedback. We would like to thank all the members of the research group “Environmental Process Engineering” (UVT) for their help and support during this study.

Appendix A. Supporting information

Supplementary data associated with this article can be found in the online version at doi:10.1016/j.jece.2024.113071.

References

[1] W. Verstraete, F. Morgan-Sagastume, S. Aiyuk, M. Waweru, K. Rabaey, G. Lissens, Anaerobic digestion as a core technology in sustainable management of organic matter, Water Sci. Technol. 52 (2005) 59–66, https://doi.org/10.2166/WST.2005.0498.
[2] M. Nikolausz, J. Kretzschmar, Anaerobic digestion in the 21st century, Bioengineering 7 (2020) 1–3, https://doi.org/10.3390/BIOENGINEERING7040157.
[3] U. Schröder, F. Harnisch, L.T. Angenent, Microbial electrochemistry and technology: terminology and classification, Energy Environ. Sci. 8 (2015) 513–519, https://doi.org/10.1039/C4EE03359K.
[4] W. Wang, D.J. Lee, Z. Lei, Integrating anaerobic digestion with microbial electrolysis cell for performance enhancement: a review, Bioresour. Technol. 344 (2022), https://doi.org/10.1016/J.BIORTECH.2021.126321.
[5] M. Cerrillo, M. Viñas, A. Bonmatí, Anaerobic digestion and electromethanogenic microbial electrolysis cell integrated system: increased stability and recovery of ammonia and methane, Renew. Energy 120 (2018) 178–189, https://doi.org/10.1016/j.renene.2017.12.062.
[6] L. Cristiani, M. Zeppilli, C. Porcu, M. Majone, Ammonium recovery and biogas upgrading in a tubular micro-pilot microbial electrolysis cell (MEC), Page 2723 25,

Molecules 2020 Vol. 25 (2020) 2723, https://doi.org/10.3390/MOLECULES25122723.
[7] K. Dolch, J. Danzer, T. Kabbeck, B. Bierer, J. Erben, A.H. Förster, J. Maisch, P. Nick, S. Kerzenmacher, J. Gescher, Characterization of microbial current production as a function of microbe-electrode-interaction, Bioresour. Technol. 157 (2014) 284–292, https://doi.org/10.1016/j.biortech.2014.01.112.
[8] E. Kipf, R. Zengerle, J. Gescher, S. Kerzenmacher, How does the choice of anode material influence electrical performance? A comparison of two microbial fuel cell model organisms, ChemElectroChem 1 (2014) 1849–1853, https://doi.org/10.1002/celc.201402036.
[9] R. Kiran, S.A. Patil, Microbial electroactive biofilms, ACS Symp. . Ser. 1323 (2019) 159–186, https://doi.org/10.1021/BK-2019-1323.CH008/ASSET/IMAGES/LARGE/BK-2019-00001K_G005.JPEG.
[10] A.A. Yaqoob, M.N.M. Ibrahim, C. Guerrero-Barajas, Modern trend of anodes in microbial fuel cells (MFCs): an overview, Environ. Technol. Innov. 23 (2021) 101579, https://doi.org/10.1016/J.ETI.2021.101579.
[11] X. Fan, Y. Zhou, X. Jin, R.B. Song, Z. Li, Q. Zhang, Carbon material-based anodes in the microbial fuel cells, Carbon Energy 3 (2021) 449–472, https://doi.org/10.1002/CEY2.113.
[12] J.M. Sonawane, A. Yadav, P.C. Ghosh, S.B. Adeloju, Recent advances in the development and utilization of modern anode materials for high performance microbial fuel cells, Biosens. Bioelectron. 90 (2017) 558–576, https://doi.org/10.1016/J.BIOS.2016.10.014.
[13] D. Pocaznoi, A. Calmet, L. Etcheverry, B. Erable, A. Bergel, Stainless steel is a promising electrode material for anodes of microbial fuel cells, Energy Environ. Sci. 5 (2012) 9645–9652, https://doi.org/10.1039/C2EE22429A.
[14] I. Vázquez, S. Kerzenmacher, Ó. Santiago, Stainless steel wool as novel bioanode for microbial electrolysis cells: a systematic study of materials, Front. Energy Res. 11 (2023) 124, https://doi.org/10.3389/FENRG.2023.1119090.
[15] D.Y.A. Esquivel, Y. Guo, R.K. Brown, S. Müller, U. Schröder, F. Harnisch, Investigating community dynamics and performance during microbial electrochemical degradation of whey, ChemElectroChem 7 (2020) 989–997, https://doi.org/10.1002/CELC.201902109.
[16] C. Koch, K.J. Huber, B. Bunk, J. Overmann, F. Harnisch, Trophic networks improve the performance of microbial anodes treating wastewater, Npj Biofilms Micro 2019 5 1 (5) (2019) 1–9, https://doi.org/10.1038/s41522-019-0100-y.
[17] E. Kipf, J. Erben, R. Zengerle, J. Gescher, S. Kerzenmacher, Systematic investigation of anode materials for microbial fuel cells with the model organism G. sulfurreducens, Bioresour. Technol. Rep. 2 (2018) 29–37, https://doi.org/10.1016/j.biteb.2018.03.005.
[18] E. Kipf, J. Koch, B. Geiger, J. Erben, K. Richter, J. Gescher, R. Zengerle, S. Kerzenmacher, Systematic screening of carbon-based anode materials for microbial fuel cells with Shewanella oneidensis MR-1, Bioresour. Technol. 146 (2013) 386–392, https://doi.org/10.1016/j.biortech.2013.07.076.
[19] B. Christgen, M. Spurr, E.M. Milner, P. Izadi, C. McCann, E. Yu, T. Curtis, K. Scott, I. M. Head, Does pre-enrichment of anodes with acetate to select for Geobacter spp. enhance performance of microbial fuel cells when switched to more complex substrates? Front. Microbiol. 14 (2023) https://www.frontiersin.org/articles/10.3389/fmicb.2023.1199286 (accessed January 31, 2024).
[20] R. Rousseau, L. Etcheverry, E. Roubaud, R. Basséguy, M.-L. Délia, A. Bergel, Microbial electrolysis cell (MEC): strengths, weaknesses and research needs from electrochemical engineering standpoint, Appl. Energy 257 (2020) 113938, https://doi.org/10.1016/j.apenergy.2019.113938.
[21] L.F.M. Rosa, C. Koch, B. Korth, F. Harnisch, Electron harvest and treatment of amendment free municipal wastewater using microbial anodes: a case study, J. Power Sources 356 (2017) 319–323, https://doi.org/10.1016/J.JPOWSOUR.2017.03.095.
[22] J. Madjarov, A. Prokhorova, T. Messinger, J. Gescher, S. Kerzenmacher, The performance of microbial anodes in municipal wastewater: pre-grown multispecies biofilm vs. natural inocula, Bioresour. Technol. 221 (2016) 165–171, https://doi.org/10.1016/j.biortech.2016.09.004.
[23] J. Kretzschmar, P. Böhme, J. Liebetrau, M. Mertig, F. Harnisch, Microbial electrochemical sensors for anaerobic digestion process control - performance of electroactive biofilms under real conditions, Chem. Eng. Technol. 41 (2018) 687–695, https://doi.org/10.1002/ceat.201700539.
[24] D. Dzofou Ngoumelah, F. Harnisch, J. Kretzschmar, Benefits of age–improved resistance of mature electroactive biofilm anodes in anaerobic digestion, Environ. Sci. Technol. 55 (2021) 8258–8266, https://doi.org/10.1021/acs.est.0c07320.
[25] P. Chatterjee, P. Dessì, M. Kokko, A.-M. Lakaniemi, P. Lens, Selective enrichment of biocatalysts for bioelectrochemical systems: a critical review, Renew. Sustain. Energy Rev. 109 (2019) 10–23, https://doi.org/10.1016/j.rser.2019.04.012.
[26] M.T. Knoll, E. Fuderer, J. Gescher, Sprayable biofilm – Agarose hydrogels as 3D matrix for enhanced productivity in bioelectrochemical systems, Biofilm 4 (2022) 100077, https://doi.org/10.1016/J.BIOFLM.2022.100077.
[27] A. Prokhorova, K. Sturm-Richter, A. Doetsch, J. Gescher, Resilience, dynamics, and interactions within a model multispecies exoelectrogenic-biofilm community, Appl. Environ. Microbiol. 83 (2017), https://doi.org/10.1128/AEM.03033-16.
[28] M.V. Coppi, C. Leang, S.J. Sandler, D.R. Lovley, Development of a Genetic System for Geobacter sulfurreducens, Applied and Environmental Microbiology 67 (2001) 3180–3187. https://doi.org/10.1128/AEM.67.7.3180-3187.2001/ASSET/6BD197AB-D071-445E–8E5F–5B408F043C87/ASSETS/GRAPHIC/AM0710174004.JPEG..
[29] J. Erben, X. Wang, S. Kerzenmacher, High current production of shewanella oneidensis with electrospun carbon nanofiber anodes is directly linked to biofilm formation**, ChemElectroChem 8 (2021) 1836–1846, https://doi.org/10.1002/CELC.202100192.
[30] J. Erben, A. Heußner, S. Thiele, S. Kerzenmacher, Activation of electrospun carbon fibers: the effect of fiber diameter on CO2 and steam reaction kinetics, J. Polym. Res. 28 (2021) 1–14, https://doi.org/10.1007/s10965-020-02386-w.
[31] J. Erben, Z.A. Pinder, M.S. Lüdtke, S. Kerzenmacher, Local acidification limits the current production and biofilm formation of shewanella oneidensis MR-1 with electrospun anodes, Front. Microbiol. 12 (2021), https://doi.org/10.3389/fmicb.2021.660474.
[32] A.M. Ziganshin, J. Liebetrau, J. Pröter, S. Kleinsteuber, Microbial community structure and dynamics during anaerobic digestion of various agricultural waste materials, Appl. Microbiol Biotechnol. 97 (2013) 5161–5174, https://doi.org/10.1007/s00253-013-4867-0.
[33] X. Zhang, Y. Wang, P. Jiao, M. Zhang, Y. Deng, C. Jiang, X.-W. Liu, L. Lou, Y. Li, X.-X. Zhang, L. Ma, Microbiome-functionality in anaerobic digesters: a critical review, Water Res. 249 (2024) 120891, https://doi.org/10.1016/j.watres.2023.120891.
[34] J.W. Lim, T. Park, Y.W. Tong, Z. Yu, Chapter One - The microbiome driving anaerobic digestion and microbial analysis, in: Y. Li, S.K. Khanal (Eds.), Advances in Bioenergy, Elsevier, 2020, pp. 1–61, https://doi.org/10.1016/bs.aibe.2020.04.001.
[35] L.N. Nguyen, A.Q. Nguyen, L.D. Nghiem, Microbial Community in Anaerobic Digestion System: Progression in Microbial Ecology, in: X.-T. Bui, C. Chiemchaisri, T. Fujioka, S. Varjani (Eds.), Water and Wastewater Treatment Technologies, Springer, Singapore, 2019, pp. 331–355, https://doi.org/10.1007/978-981-13-3259-3_15.
[36] J. Madjarov, S.C. Popat, J. Erben, A. Götze, R. Zengerle, S. Kerzenmacher, Revisiting methods to characterize bioelectrochemical systems: the influence of uncompensated resistance (iRu-drop), double layer capacitance, and junction potential, J. Power Sources 356 (2017) 408–418, https://doi.org/10.1016/J.JPOWSOUR.2017.03.033.
[37] P.J. Mohr, B.N. Taylor, D.B. Newell, CODATA recommended values of the fundamental physical constants: 2006, Rev. Mod. Phys. 80 (2008) 633–730, https://doi.org/10.1103/RevModPhys.80.633.
[38] M.S.M. Jetten, A.J.M. Stams, A.J.B. Zehnder, Methanogenesis from acetate: a comparison of the acetate metabolism in Methanothrix soehngenii and Methanosarcina spp, FEMS Microbiol. Rev. 8 (1992) 181–197, https://doi.org/10.1111/j.1574-6968.1992.tb04987.x.
[39] H. Min, S.H. Zinder, Kinetics of acetate utilization by two thermophilic acetotrophic methanogens: methanosarcina sp. Strain CALS-1 and Methanothrix sp. Strain CALS-1, Appl. Environ. Microbiol 55 (1989) 488–491.
[40] J. Kretzschmar, C. Koch, J. Liebetrau, M. Mertig, F. Harnisch, Electroactive biofilms as sensor for volatile fatty acids: cross sensitivity, response dynamics, latency and stability, Sens. Actuators, B: Chem. 241 (2017) 466–472, https://doi.org/10.1016/j.snb.2016.10.097.
[41] H. Horn, S. Wäsche, D.C. Hempel, Simulation of biofilm growth, substrate conversion and mass transfer under different hydrodynamic conditions, Water Sci. Technol. 46 (2002) 249–252.
[42] S. Wäsche, H. Horn, D.C. Hempel, Mass transfer phenomena in biofilm systems, Water Sci. Technol. 41 (2000) 357–360, https://doi.org/10.2166/wst.2000.0466.
[43] S. Wäsche, H. Horn, D.C. Hempel, Influence of growth conditions on biofilm development and mass transfer at the bulk/biofilm interface, Water Res. 36 (2002) 4775–4784, https://doi.org/10.1016/S0043-1354(02)00215-4.
[44] H.-C. Flemming, J. Wingender, The biofilm matrix, Nat. Rev. Microbiol 8 (2010) 623–633, https://doi.org/10.1038/nrmicro2415.
[45] H.-C. Flemming, J. Wingender, U. Szewzyk, P. Steinberg, S.A. Rice, S. Kjelleberg, Biofilms: an emergent form of bacterial life, Nat. Rev. Microbiol 14 (2016) 563–575, https://doi.org/10.1038/nrmicro.2016.94.
[46] H.-C. Flemming, T.R. Neu, D.J. Wozniak, The EPS Matrix: the "House of Biofilm Cells, J. Bacteriol. 189 (2007) 7945–7947, https://doi.org/10.1128/jb.00858-07.
[47] H.-C. Flemming, J. Wingender, Relevance of microbial extracellular polymeric substances (EPSs) - Part I: structural and ecological aspects, Water Sci. Technol. 43 (2001) 1–8, https://doi.org/10.2166/wst.2001.0326.
[48] J.P. Kotzé, P.G. Thiel, W.H.J. Hattingh, Anaerobic digestion II. The characterization and control of anaerobic digestion, Water Res. 3 (1969) 459–494, https://doi.org/10.1016/0043-1354(69)90014-1.
[49] Y. Rafrafi, L. Laguillaumie, C. Dumas, Biological Methanation of H2 and CO2 with Mixed Cultures: current advances, hurdles and challenges, Waste Biomass-.-. Valor 12 (2021) 5259–5282, https://doi.org/10.1007/s12649-020-01283-z.
[50] Z. He, Y. Huang, A.K. Manohar, F. Mansfeld, Effect of electrolyte pH on the rate of the anodic and cathodic reactions in an air-cathode microbial fuel cell, Bioelectrochemistry 74 (2008) 78–82, https://doi.org/10.1016/j.bioelechem.2008.07.007.
[51] Y. Yuan, B. Zhao, S. Zhou, S. Zhong, L. Zhuang, Electrocatalytic activity of anodic biofilm responses to pH changes in microbial fuel cells, Bioresour. Technol. 102 (2011) 6887–6891, https://doi.org/10.1016/j.biortech.2011.04.008.
[52] E. Maleki, A. Bokhary, B.Q. Liao, A review of anaerobic digestion bio-kinetics, Rev. Environ. Sci. Biotechnol. 17 (2018) 691–705, https://doi.org/10.1007/s11157-018-9484-z.
[53] T.H. Nguyen, M.K. Nguyen, T.H.O. Le, T.T. Bui, T.H. Nguyen, T.Q. Nguyen, A. van Ngo, Kinetics of organic biodegradation and biogas production in the pilot-scale moving bed biofilm reactor (MBBR) for piggery wastewater treatment, J. Anal. Methods Chem. 2021 (2021) 6641796, https://doi.org/10.1155/2021/6641796.
[54] G. Zellner, F. Neudörfer, H. Diekmann, Degradation of lactate by an anaerobic mixed culture in a fluidized-bed reactor, Water Res. 28 (1994) 1337–1340, https://doi.org/10.1016/0043-1354(94)90299-2.
[55] C.A. Contreras-Dávila, A. Ali, C.J.N. Buisman, D.P.B.T.B. Strik, Lactate Metabolism and Microbiome Composition Are Affected by Nitrogen Gas Supply in Continuous

Lactate-Based Chain Elongation, Fermentation 7 (2021) 41, https://doi.org/10.3390/fermentation7010041.
[56] M. Mannaa, G. Han, Y.-S. Seo, I. Park, Evolution of food fermentation processes and the use of multi-omics in deciphering the roles of the microbiota, Foods 10 (2021) 2861, https://doi.org/10.3390/foods10112861.
[57] J. Li, Q. Ban, L. Zhang, ajay kumar Jha, Syntrophic propionate degradation in anaerobic digestion: a review, Int. J. Agric. Biol. 14 (2012) 843–850.
[58] L. Moreno, M. Nemati, B. Predicala, Biokinetic evaluation of fatty acids degradation in microbial fuel cell type bioreactors, Bioprocess Biosyst. Eng. 38 (2015) 25–38, https://doi.org/10.1007/s00449-014-1240-3.
[59] M. Harb, N. Ermer, C.B. Sawaya, A.L. Smith, Increased applied voltage in the presence of GAC enhances microbial activity and methane production during anaerobic digestion of food waste, Environ. Sci.: Water Res. Technol. 6 (2020) 737–746, https://doi.org/10.1039/C9EW01000A.
[60] Z. Yu, X. Leng, S. Zhao, J. Ji, T. Zhou, A. Khan, A. Kakde, P. Liu, X. Li, A review on the applications of microbial electrolysis cells in anaerobic digestion, Bioresour. Technol. 255 (2018) 340–348, https://doi.org/10.1016/j.biortech.2018.02.003.
[61] W. Liu, W. Cai, Z. Guo, L. Wang, C. Yang, C. Varrone, A. Wang, Microbial electrolysis contribution to anaerobic digestion of waste activated sludge, leading to accelerated methane production, Renew. Energy 91 (2016) 334–339, https://doi.org/10.1016/j.renene.2016.01.082.
[62] C. Engel, F. Schattenberg, K. Dohnt, U. Schröder, S. Müller, R. Krull, Long-term behavior of defined mixed cultures of geobacter sulfurreducens and Shewanella oneidensis in bioelectrochemical systems, Front. Bioeng. Biotechnol. 7 (2019), https://doi.org/10.3389/FBIOE.2019.00060.
[63] A.G. Chioti, V. Tsioni, S. Patsatzis, E. Filidou, D. Banti, P. Samaras, E.A. Economou, E. Kostopoulou, T. Sfetsas, Characterization of biofilm microbiome formation developed on novel 3d-printed zeolite biocarriers during aerobic and anaerobic digestion processes, Fermentation 8 (2022) 746, https://doi.org/10.3390/fermentation8120746.
[64] P. Świątczak, A. Cydzik-Kwiatkowska, P. Rusanowska, Microbiota of anaerobic digesters in a full-scale wastewater treatment plant, Arch. Environ. Prot. 43 (2017) 53–60, https://doi.org/10.1515/aep-2017-0033.
[65] A.G. Talavera-Caro, I.O.H.-D. Lira, E.R. Cruz, M.A. Sánchez-Muñoz, N. Balagurusamy, The Realm of Microorganisms in Biogas Production: Microbial Diversity, Functional Role, Community Interactions, and Monitoring the Status of Biogas Plant, in: N. Balagurusamy, A.K. Chandel (Eds.), Biogas Production: From Anaerobic Digestion to a Sustainable Bioenergy Industry, Springer International Publishing, Cham, 2020, pp. 179–212, https://doi.org/10.1007/978-3-030-58827-4_10.
[66] I. Maus, D.E. Koeck, K.G. Cibis, S. Hahnke, Y.S. Kim, T. Langer, J. Kreubel, M. Erhard, A. Bremges, S. Off, Y. Stolze, S. Jaenicke, A. Goesmann, A. Sczyrba, P. Scherer, H. König, W.H. Schwarz, V.V. Zverlov, W. Liebl, A. Pühler, A. Schlüter, M. Klocke, Unraveling the microbiome of a thermophilic biogas plant by metagenome and metatranscriptome analysis complemented by characterization of bacterial and archaeal isolates, Biotechnol. Biofuels 9 (2016) 171, https://doi.org/10.1186/s13068-016-0581-3.
[67] M.K. Nobu, T. Narihiro, R. Mei, Y. Kamagata, P.K.H. Lee, P.-H. Lee, M. J. McInerney, W.-T. Liu, Catabolism and interactions of uncultured organisms shaped by eco-thermodynamics in methanogenic bioprocesses, Microbiome 8 (2020) 111, https://doi.org/10.1186/s40168-020-00885-y.
[68] D. Rivière, V. Desvignes, E. Pelletier, S. Chaussonnerie, S. Guermazi, J. Weissenbach, T. Li, P. Camacho, A. Sghir, Towards the definition of a core of microorganisms involved in anaerobic digestion of sludge, ISME J. 2009 3 6 (3) (2009) 700–714, https://doi.org/10.1038/ismej.2009.2.
[69] F. Caccavo, D.J. Lonergan, D.R. Lovley, M. Davis, J.F. Stolz, M.J. McInerney, Geobacter sulfurreducens sp. nov., a hydrogen- and acetate-oxidizing dissimilatory metal-reducing microorganism, Appl. Environ. Microbiol. 60 (1994) 3752–3759, https://doi.org/10.1128/aem.60.10.3752-3759.1994.
[70] E. Perman, A. Schnürer, A. Björn, J. Moestedt, Serial anaerobic digestion improves protein degradation and biogas production from mixed food waste, Biomass-.-. Bioenergy 161 (2022) 106478, https://doi.org/10.1016/j.biombioe.2022.106478.
[71] J. Lee, E. Kim, G. Han, J.V. Tongco, S.G. Shin, S. Hwang, Microbial communities underpinning mesophilic anaerobic digesters treating food wastewater or sewage sludge: a full-scale study, Bioresour. Technol. 259 (2018) 388–397, https://doi.org/10.1016/j.biortech.2018.03.052.
[72] T. Yamada, Y. Sekiguchi, S. Hanada, H. Imachi, A. Ohashi, H. Harada, Y. Kamagata, Anaerolinea thermolimosa sp. nov., Levilinea saccharolytica gen. nov., sp. nov. and Leptolinea tardivitalis gen. nov., sp. nov., novel filamentous anaerobes, and description of the new classes Anaerolineae classis nov. and Caldilineae classis nov. in the bacterial phylum Chloroflexi, Int. J. Syst. Evol. Microbiol 56 (2006) 1331–1340, https://doi.org/10.1099/ijs.0.64169-0.
[73] R.D.A. Cayetano, J. Park, G.-B. Kim, J.-H. Jung, S.-H. Kim, Enhanced anaerobic digestion of waste-activated sludge via bioaugmentation strategy—Phylogenetic investigation of communities by reconstruction of unobserved states (PICRUSt2) analysis through hydrolytic enzymes and possible linkage to system performance, Bioresour. Technol. 332 (2021) 125014, https://doi.org/10.1016/j.biortech.2021.125014.
[74] D. Pérez-Pantoja, R. Donoso, L. Agulló, M. Córdova, M. Seeger, D.H. Pieper, B. González, Genomic analysis of the potential for aromatic compounds biodegradation in Burkholderiales, Environ. Microbiol. 14 (2012) 1091–1117, https://doi.org/10.1111/j.1462-2920.2011.02613.x.
[75] B. Demirel, P. Scherer, The roles of acetotrophic and hydrogenotrophic methanogens during anaerobic conversion of biomass to methane: a review, Rev. Environ. Sci. Biotechnol. 7 (2008) 173–190, https://doi.org/10.1007/s11157-008-9131-1.
[76] I. Anderson, L.E. Ulrich, B. Lupa, D. Susanti, I. Porat, S.D. Hooper, A. Lykidis, M. Sieprawska-Lupa, L. Dharmarajan, E. Goltsman, A. Lapidus, E. Saunders, C. Han, M. Land, S. Lucas, B. Mukhopadhyay, W.B. Whitman, C. Woese, J. Bristow, N. Kyrpides, Genomic characterization of methanomicrobiales reveals three classes of methanogens, PLOS ONE 4 (2009) e5797, https://doi.org/10.1371/journal.pone.0005797.
[77] D.R. Lovley, Happy together: microbial communities that hook up to swap electrons, ISME J. 11 (2017) 327–336, https://doi.org/10.1038/ismej.2016.136.